HHS Public Access

Author manuscript

Nat Cell Biol. Author manuscript; available in PMC 2012 June 28.

Published in final edited form as:

Nat Cell Biol. 2010 December ; 12(12): 1228–1234. doi:10.1038/ncb2127.

A Cytoplasmic Dynein Tail Mutation Impairs Motor Processivity

Kassandra M. Ori-McKenney[1,2,4], **Jing Xu**[3,4], **Steven P. Gross**[3,5], and **Richard B. Vallee**[1,2,5]

[1]Department of Pathology and Cell Biology, Columbia University. New York, New York 10032.

[2]Department of Biological Sciences, Columbia University, New York, New York 10027.

[3]Department of Developmental and Cell Biology, University of California, Irvine. Irvine California 92697.

Abstract

Mutations in the tail of the cytoplasmic dynein molecule have been reported to cause neurodegenerative disease in mice. The mutant mouse strain Legs at Odd Angles (Loa) exhibits impaired retrograde axonal transport, but the molecular deficiencies in the mutant dynein molecule, and how they contribute to neurodegeneration, are unknown. To address these questions, we purified wild-type and mutant mouse dynein. Using biochemical, single molecule, and live cell imaging techniques, we find a strong inhibition of motor run-length *in vitro* and *in vivo*, and significantly altered motor domain coordination in the mutant dynein. These results suggest a potential role for the dynein tail in motor function, and provide the first direct evidence for a link between single-motor processivity and disease.

Cytoplasmic dynein is a minus-end directed microtubule motor protein responsible for a variety of cellular functions, including retrograde axonal transport[1]. Two dynein mutant mouse strains, Legs at Odd Angles (Loa) and Cramping1 (Cra1), were identified in a screen for genes involved in late onset motor neuron disease (MND)[2]. This finding identified a new class of MND genes, which also includes the mouse and human p150*Glued* gene encoding a subunit of the dynein regulatory complex dynactin[3–5], and significantly expanded the limited pool of familial Amyotrophic Lateral Sclerosis (ALS) candidate genes. Of the dynein mutations, Loa has received particular attention[6–10]. Loa/+ mice were initially reported to exhibit lower motor neuron degeneration, but more recent studies have found severe loss of sensory neurons[8,9]. Loa mutant mice also exhibited a decreased rate of

Correspondence should be addressed to R.B.V. and S.P.G. Dr. Richard B. Vallee, Ph.D., Department of Pathology and Cell Biology, Columbia University, Physicians and Surgeons Building, Room 15-409, 630 West 168th Street, New York, NY 10032, Phone: 212-342-0546, rv2025@columbia.edu or Dr. Steven P. Gross, Ph.D., Department of Developmental and Cell Biology, University of California, Irvine, 2222 Natural Sciences 1, Irvine, CA 92697, Phone: 949-824-3159, sgross@uci.edu.

[4]These authors contributed equally to this work

[5]Co-senior authors

Author Contributions

KMOM, JX, SPG, and RBV designed the research. KMOM and JX performed experiments and analyzed data. KMOM, JX, SPG, and RBV wrote the paper.

Competing Interests Statement

The authors declare no competing financial interests.

retrograde axonal transport[2,10]. The Loa mutation resides in the extreme N-terminal region of the dynein heavy chain (HC) polypeptide (F580Y), within the dynein "tail." This region is responsible for organizing the multiple dynein subunits into a complex and for binding to membranous cargo. Dynein generates force through its two motor domains, each located at the C-terminal end of the HC, 1,500 a.a. (15–20 nm) away from the site of the Loa mutation. Whether and how the Loa mutation affects cytoplasmic dynein function has remained untested.

To approach this problem, we first tested the ability of Loa mutant dynein to remain associated with membranous vesicles isolated by sucrose step gradient flotation from wild-type, Loa/+ and Loa/Loa brains, but found no clear difference (Fig. 1a). The Loa mutation lies in the region of the dynein HC involved in HC-HC dimerization and in HC-intermediate chain (IC) binding (Supplementary Information, Fig. S1). We therefore tested for potential defects in the stability of the mutant complex. Fractionation of whole brain cytosol by sucrose density gradient centrifugation revealed a single major 20S dynein peak for both the wild-type and Loa/+ mutant animals. Loa/Loa dynein, in contrast, showed a small but reproducible decrease in dynein s-value, accompanied by the appearance of a free IC peak (12 ± 2 % of total ICs) at 6S (Supplementary Information, Fig. S2a). To test whether these observations reflect a more general reduction in mutant dynein stability, we exposed brain extracts to potassium iodide (KI), a chaotropic salt to which dynein is particularly sensitive[11]. In the presence of KI, dynein dissociation increased both as a function of KI concentration and of the proportion of mutant dynein HC (Supplementary Information, Fig. S2b–d). These results indicate that the Loa mutation may impair the interactions between subunits.

To gain further insight into the molecular effects of the Loa mutation, we purified cytoplasmic dynein from wild-type and Loa/+ adult mouse brains[1]. As we observed in brain cytosol, the purified mutant dynein remained intact by sucrose density gradient centrifugation (data not shown). The purified Loa/+ dynein showed no differences in subunit composition from the wild-type mouse protein, and neither preparation showed detectable levels of the processivity factor dynactin by Coomassie Blue staining or immunoblotting (Fig. 1b; Supplementary Information, Fig. S3a–b). Because the homozygous mutant mice die shortly after birth, the amounts of brain tissue we could obtain were inadequate to purify biochemical amounts of dynein by this procedure. Nonetheless, we were still able to purify small amounts of Loa/Loa dynein for single molecule analysis using a modification of this method (Fig. 2–3, Supplementary Information, Fig. S3c–d).

To test the effects of the Loa mutation on dynein mechanochemical activity, we measured the ATPase activity of wild-type and Loa/+ dynein in the presence and absence of microtubules. The basal ATPase activity was similar for both wild-type and Loa/+ dynein: 51.3 ± 5.3 and 51.7 ± 3.3 nmole Pi/min/mg, respectively (Fig. 1c). However, in the presence of microtubules, the ATPase activities of wild-type and mutant dynein differed markedly. The Michaelis constant for microtubules, K_{mMT}, was 1.5 ± 0.2 μM for the purified wild-type dynein, similar to the value for bovine cytoplasmic dynein[12], whereas the K_{mMT} for Loa/+ dynein was considerably higher, 11.8 ± 3.4 μM (P<0.001). In contrast, the maximum rate (V_{max}) values were very similar (wild-type = 255 ± 9 nmol/min/mg; Loa/+ = 263 ± 43

nmol/min/mg). The latter results indicate that the maximal ATP turnover rate is unaffected by the Loa mutation. The increased K_{mMT}, however, suggests a pronounced decrease in the effective affinity of the mutant dynein for microtubules during ATP hydrolysis. In support of this possibility, the K_{mMT} for Loa/+ was partially rescued at reduced ionic strength (4.0 ± 0.6 μM *vs.* 1.2 ± 0.2 μM for wild-type), which increases dynein-microtubule affinity[12]. Furthermore, microtubule binding by the purified mutant dynein was markedly reduced relative to wild-type dynein in the presence of ATP, though not in its absence (apo state) (Fig. 1d). This surprising result suggests that much of the dynein fraction normally seen to cosediment with microtubules in the presence of ATP is engaged in active, processive movement along the microtubule. These results together suggest an effect of the Loa mutation on the interaction of dynein with microtubules during the ATPase and force-generating portion of the crossbridge cycle, though not in the strong microtubule binding (apo) state.

To gain insight into the underlying molecular defects, we used quantum dot and optical trap assays under single molecule conditions. We attached dynein to quantum dots using antibodies to the tail of the wild-type and mutant molecules and analyzed their velocity and run-length. Movements in the two dynein preparations were ATP-dependent and at a velocity similar to that reported for mouse dynein-dynactin complexes (Fig. 2a; Supplementary Information, Fig. S4a)[13]. The purified wild-type and mutant dyneins showed predominantly unidirectional movements, but some bidirectional events were also observed, as previously reported (Fig. 2c)[13–15]. A clear difference, however, was observed in the wild-type *vs*. mutant dynein run-lengths (Fig. 2b–c). Wild-type dynein exhibited an average run-length of 339 ± 33 nm (Fig. 2c), about half that of mouse dynein-dynactin complexes[13], a reflection of the absence of dynactin from our dynein preparations. Loa/+ dynein displayed fewer long runs and a 23 % shorter average run-length (259 ± 9 nm). Loa/Loa dynein was even more impaired, with an average run-length approximately half that of wild-type dynein (175 ± 4 nm) (Fig. 2c). Optical trap experiments using the same dynein preparations adsorbed to polystyrene beads gave comparable results, with no difference in average velocity between Loa/+ and wild-type dynein, but with a similar reduction in Loa/+ single motor processivity (Fig. 3a; Supplementary Information, Fig. S4b–c). Based on the motility data, we calculate a 31–37 % increase in the average off-rate for Loa/+ *vs.* wild-type dynein at 0.5 – 1 mM ATP, respectively (see Supplementary Information), consistent with the enhanced dissociation of Loa/+ dynein from microtubules in the presence of ATP (Fig. 1). As for bovine cytoplasmic dynein, the stall force for single wild-type mouse dynein molecules was 1.4 ± 0.3 pN, and within experimental error of those measured for Loa/+ (1.7 ± 0.4 pN) and Loa/Loa dynein (1.6 ± 0.4 pN) (Fig. 3b)[14,16]. We also observed no difference in the step size of the wild-type or mutant dynein motors while they moved along microtubules under load (Fig. 3c; Supplementary Information, Fig. S5a–c).

Physiological cargoes typically use multiple motors. To assess how the observed defects in dynein processivity translate to the *in vivo* condition, we tested the run-lengths for multiple wild-type and Loa mutant dyneins *in vitro* and found an increase in run-length for multi-motor conditions (as reported in [17]); however, this increase was attenuated for the Loa/+ dynein (Fig. 3d). We also carried out computational modeling of dynein run-lengths at more

extensive motor/cargo ratios, and found the mean travel defect to persist to three or more dynein molecules/cargo, with and without assuming potential effects of *in vivo* factors such as dynactin[13,18,19] (Fig. 4b; Supplementary Information, Fig. S6a–b). We find here that an additional consequence of decreased single molecule processivity is a reduction in the number of instantaneously engaged motors per cargo in the multiple motor range, which in turn further limits cargo travel (Fig. S6b). These simulations reveal a previously unappreciated sensitivity of multiple-motor run-lengths to changes in single-motor processivity, especially apparent here where the single-motor processivity is low in comparison to bovine dynein.

The Loa mutation has been linked to defects in retrograde axonal transport[2]. To compare the effects of the Loa mutation *in vivo* with our *in vitro* data, we performed live cell imaging analysis of lysosome/late endosome behavior at high temporal resolution (5 frames/sec; Fig. 4a–c). We then used custom analysis software to precisely identify periods of uninterrupted motion ("runs", see Supplemental Information). We imaged the far distal region of the axon (>100 um from cell body), where we observed predominantly unidirectional, retrograde runs as previously described[20]. Retrograde run-lengths were reduced by 53 % and 83 % in Loa/+ and Loa/Loa neurons, respectively (Fig. 4b; Supplementary Information, Fig. S6c). The wild-type *in vivo* run-length (5.27 ± 0.34 μm) allowed us to use our theoretical model to estimate an average of 7.7 dynein molecules per cargo (Fig. 4b), similar to recent values based on stall force and biochemical isolation[21,22]. We then predicted the expected mutant run-lengths at the same 7.7 dyneins/cargo, adjusting only the single-motor processivity to reflect the measured *in vitro* processivity defects. The predicted run-lengths were in excellent agreement with those measured *in vivo* (2.49 ± 0.13 vs. 2.43 ± 0.21 μm for Loa/+; 0.89 ± 0.05 vs. 0.86 ± 0.07 μm for Loa/Loa, Fig. 4b). As in our *in vitro* experiments (Fig. 2–3), we see no change in instantaneous lysosome velocity in the Loa mutant neurons (Fig. 4c, left). However, the overall average velocity was reduced by 22 % in Loa/+ and 43 % in Loa/Loa neurons *vs.* wild-type (Fig. 4c, right), consistent with an increase in run terminations, and comparable to theoretical prediction (11 % decrease in average velocity for Loa/+ and 37 % for Loa/Loa, see Supplemental Information). Together, these results argue strongly that the Loa dynein processivity defect we identify *in vitro* can account for the observed impairment in retrograde axonal transport.

To gain further insight into the mechanism responsible for altered Loa dynein processivity, we tested for the reported tendency of cytoplasmic dynein to step laterally on the microtubule surface, in contrast to the strict linear travel of kinesin[15,23]. We confirmed lateral stepping in mouse dynein, and observed a significant increase in its frequency for the Loa/+ mutant protein (Fig. 5a–b). One potential explanation for this result is a disrupted coordination between the two motor domains within the native dynein complex. A gating mechanism between dimeric motor domains is well established for kinesins and myosins, but is not well understood for dynein[24–26]. Gating contributes to processive motion by ensuring that, as one motor domain advances, the other remains strongly associated with its track in the apo state, thereby preventing premature detachment[26]. As a test for altered gating in the Loa mutant dynein, we measured its K_{mATP}. Despite the somewhat decreased V_{max} for Loa/+ dynein due to its lower K_{mMT} (Fig. 1c), the K_{mATP} was clearly decreased

(18.8 ± 4.1 μM *vs.* 27.0 ± 6.5 μM for wild-type, $P<0.05$) (Fig. 5c). This result is consistent with a defect in communication between motor domains, allowing premature ATP binding by the apo motor domain, and subsequent release from the microtubule (Fig. 5d), though further kinetic analysis will be needed to confirm this model.

These results have novel implications for intramolecular regulation of cytoplasmic dynein motor activity. Despite the location of the Loa mutation within the dynein tail, we find several lines of evidence for an altered interaction between dynein and microtubules, the first direct indication for communication between the dynein motor and tail domains. The clear defect we observed in mutant dynein processivity raised the possibility of motor domain miscoordination. Supporting this, we identified novel defects in the Loa mutant dynein: both an increase in lateral stepping on the microtubule lattice, and an increased affinity for ATP apparently leading to premature run termination. Consistent with the subtly decreased stability of the Loa dynein complex, we propose that an abnormal linkage within the base of the Loa dynein molecule disrupts coordination between the two motor domains by altering their relative positioning and ability to interact laterally.

Our results also suggest a novel role for processivity defects in disease causation. We argue that neurodegeneration in the Loa/+ mutant mouse is unlikely to result from dynein subunit dissociation, which we do not detect for the Loa/+ complex in cytosolic extracts or following purification. (Only dynein from the Loa/Loa mouse, which dies shortly after birth, shows evidence of dissociation: Supplementary Information, Fig. S2). Our data also argue against a loss in the association of dynein with membranous cargo, which persisted in our biochemical analysis. The most dramatic change we observed to result from the Loa mutation was a decrease in dynein run-length. This effect quantitatively accounted for the observed defect in axonal transport as indicated by a combination of empirical analysis with computational modeling. The neurons that are most likely to be affected by this defect in processivity and impairment in transport would be those with the longest axons, such as motor and sensory neurons. Our study therefore provides the first evidence that altered motor protein processivity can have pronounced consequences for *in vivo* transport, the impairment of which clearly correlates with neuronal death and disease.

Materials and Methods

Protein Purification

Cytoplasmic dynein was purified from wild-type and Loa/+ adult brains by microtubule-affinity, ATP release, and sucrose density gradient fractionation as previously described[1]. For purification of dynein from postnatal day zero (P0) brains, cytosol from three P0 brains was subjected to sucrose density gradient fractionation, microtubule-affinity in the presence of GTP (to remove kinesin), then ATP extraction to release dynein (Fig. S3c–d).

Sucrose Density Gradients

Whole brain cytosol from P0 mice was fractionated on a 5–20 % Tris-KCl sucrose gradient (20 mM Tris-HCl, pH 7.6, 50 mM KCl, 5 mM MgSO4, 0.5 mM EDTA), or was incubated with 0.075 M, 0.15 M, or 0.30 M potassium iodide (KI) on ice for 1 hour, then fractionated

on a sucrose gradient containing 0.075 M, 0.15 M, or 0.30 M KI. Fractions were analyzed by SDS-PAGE and western blot probing for dynein heavy chain (HC)[27] (1:1000) and dynein intermediate chain (IC) (1:3000; clone 74.1, K. Pfister, University of Virginia). A solution of thyroglobulin, ferritin, catalase, lactate dehydrogenase, and albumin was fractionated on a sucrose gradient to determine S-values for the gradient fractions.

Biochemical Assays

ATPase assays were performed using the malachite green method as previously described[12] in Tris-KCl buffer containing 10 mM KCl or 50 mM KCl, and incubated at 37°C for 15 minutes in the presence of 1 mM ATP. For ATPase activity as a function of microtubules, taxol-stabilized microtubules (Cytoskeleton, Inc., Denver CO) were added to a solution containing 1 μg of dynein before adding ATP to start the reaction. For ATPase activity as a function of ATP, all reactions were performed in Tris-KCl buffer containing 10 mM KCl and in the presence of 10 μM microtubules. Activities were plotted at the range of microtubule or ATP concentrations. Michaelis-Menten curves were fit to the data to derive K_m and V_{max} values.

For microtubule binding experiments, 1 μg of dynein was incubated with a 2.5 μM final concentration of taxol stabilized microtubules at 37°C for 15 minutes, then centrifuged. Supernatant and microtubule pellet were either recovered for analysis, or the pellet was resuspended in Tris-KCl buffer containing 10 mM ATP, incubated at 37°C for 15 minutes, and centrifuged. Supernatants and pellets were analyzed by SDS-PAGE and western blot probing for dynein intermediate chain and tubulin (1:5000; Sigma).

Membrane flotation analysis was performed as previously described[10]. Briefly, two P0 brains from each genotype were homogenized and centrifuged at 30,000 g. The supernatant was centrifuged at 150,000 g. The high-speed pellet was fractionated by flotation through a 2M, 1.5M, and 0.6M sucrose step gradient. Membrane vesicles floated to the 0.6–1.5M interface. Samples were taken from the 0.6M layer, the vesicle (V) interface, and the 1.5M layer for SDS-PAGE and western blot analysis, probing for IC, HC, and synaptotagmin (1:500; StressGen) as a marker for vesicles.

Quantum Dot Assays

In vitro motility assays were conducted in flow chambers assembled from a glass slide and acid washed cover slip using double-sided adhesive tape (chamber volume ~10 μL). Solutions were incubated in the chamber for 10 minutes. The chamber was incubated with 5 mg/mL Biotin-BSA, washed 2 × 20 μL with blocking buffer (30 mM HEPES pH 7.2, 50 mM KAcetate, 2 mM MgAcetate, 1 mM EGTA, 10 % glycerol, 1 mg/ml BSA, 1 mg/ml casein), incubated with 5 mg/mL streptavidin solution, washed twice, then incubated with rhodamine- and biotin-labeled microtubules and washed twice again with blocking buffer with 5 μM taxol.

Monoclonal anti-74.1 IC antibody (350 nM), polyclonal anti-HC antibody (450 nM), or polyclonal anti-R1B2 antibody (450 nM) was mixed with goat anti-mouse or goat anti-rabbit quantum dots (QD) (350 nM) (Invitrogen) in blocking buffer for 30 minutes on ice.

Different antibodies gave similar results. Dynein (10 nM) was added to the antibody-QD mixture and incubated on ice for 30 minutes. Similar results were obtained at 1:50 protein-to-QD ratios. The dynein-QD mixture was diluted 50 times immediately prior to chamber incubation, then washed twice. Blocking buffer containing 500 μM ATP, 5 μM taxol, and an oxygen scavenging system was flowed into the chamber. Differences in run-lengths and velocities between optical trap and QD assays were due to differences in ATP concentrations. Single QD-labeled-dynein molecules were visualized at 25°C on an inverted microscope (DMIRBE, Leica) using a Qdot 525 filter set (Omega Optical, Brattleboro, Vermont). Images were captured on a CCD camera (CoolSnap HQ, Photometrics) at 5 frames/sec. The movement of individual dynein-QDs was analyzed using a custom-tracking program (Gross Lab) to identify the QD position vs. time via 2-d Gaussian fitting of their brightness profile. A processive run is defined here as motion >200 nm that is terminated by detachment from the microtubule. A bidirectional run is a >200 nm run in one direction, then a >200 nm run in the opposite direction. In the case of a bidirectional run, the run-length was measured as the sum of processive run-lengths in both directions.

Optical Trapping Experiments

Optical trap assays, data recording, particle tracking, and stalling force analysis was performed as previously described[14,28–30]. Dynein was attached directly to polystyrene beads (PolySciences, Inc.); using antibody as a linker impaired the motile behavior of beads. Bead-microtubule binding fraction was used as a read-out for the average number of available motors per bead: 50–100 % binding fractions correspond to the few motor condition, whereas ≤ 30 % binding fractions correspond to the single motor range[14,31,32]. Dynein-coated beads were positioned above a microtubule for 20–30 seconds using an optical trap. A binding event was scored upon bead binding and processive motion along microtubule. Motility and stalling force measurements were conducted using 500 nm polystyrene beads in assay buffer (10 mM PIPES, 2 mM MgSO4, 1 mM EGTA, 1 mM DTT, 50 mM K-Acetate, 10 % Glycerol, pH 6.9) supplemented with scavenging solution and 1 mM ATP immediately before measurements. An automated program monitored the bead position, then turned off the trap upon detection of processive bead motion. An individual run was defined as the course between a bead binding to, and then detaching from a microtubule. For stall force measurements, a trap stiffness of 2.2 pN/100 nm was used. A stall was scored if the bead proceeded away from trap center and held its plateau position for >300 ms before detachment.

Step size analysis was carried out on continuous segments of force traces where the systematic noise was no greater than ~8 nm, using an objective, model-independent step detection method,[33] cross verified using a chi-square reduction method,[34] and tested for kinesin stepping *in vitro*[35].

Lateral position experiments were conducted using 200 nm beads[23] in assay buffer with scavenging solution and 0.2 mM ATP. We examined dynein's lateral wandering by quantifying the change in a bead's lateral position between subsequent frames. Runs longer than 200 nm and 2 sec were analyzed. To limit possible bias toward longer travels, runs for each genotype were grouped into five different travel ranges (increment in 100 nm from 200

to >600 nm). The final distribution of lateral changes describes the mean ± SD from averaging each subgroup.

Modeling of Multiple Motor Conditions

We adapted a recently developed Monte Carlo model, which closely reproduced force measurements for multiple dyneins *in vitro*[16], constrained by our experimental measurements of single-motor processivity for wild-type, Loa/+, and Loa/Loa dyneins. A "run" is initiated when at least one of the N motors becomes stochastically bound to the microtubule (characterized by on-rate), and terminated when all N motors become detached (characterized by off-rate). For each motor, we used the same dynein stiffness (0.32 pN/nm), viscosity (10^{-3} N·sec/m^2), on-rate estimation (1/sec), step size (8 nm), as well as formulas for stepping direction, velocity, and off-rate under load as described in[16]. Dynein's off-rate under no load was the lone adjusted parameter in our simulation, and was assumed to represent the sole differentiating factor between each genotype. To estimate the appropriate off-rate (under no load) for each genotype *in vivo*, we evaluated the average run-length *in vitro* when only one motor was available for transport. To account for potential *in vivo* factors, we carried out simulations assuming a two-fold processivity enhancement of dynactin[18,19], and a 0.1 pN constant opposing force to account for viscous drag in cytosol.

Live Cell Imaging of Lysosomes

Hippocampal neurons were cultured from E19 mouse embryos as previously described and cultured for 4–6 DIV (days *in vitro*)[36]. Mice were cared for and treated according to IACUC regulations. For experiments, cultures were incubated in fresh media containing 500 μM lysotracker, washed, then imaged in 2 mL of fresh media (with 10 mM Hepes) at 37°C with 5 % CO_2 on an Olympus IX81 inverted microscope. Images were captured at 5 frames/sec for 1.5 minutes using an Hamamatsu ORCA-R2 CCD camera. Experiments were performed at least three times per genotype. For velocity, the motions of single lysosomes were analyzed using kymographs generated with the "Multiple Kymograph" plug-in for ImageJ (EMBL, Heidelberg, Germany). For run-length, individual lysosomes were identified by a 2-d Gaussian fitting of their brightness profile, and custom analysis routines identified periods of un-interrupted motion (runs), where net travel for any three consecutive frames (400 ms) was at least 80 nm in the minus-end direction.

Statistical methods

Travel distributions were fit to a single exponential decay to extract the decay constant (and fit uncertainty) as its characteristic run-length. Speed distributions were fit to a Gaussian function to extract the mean peak position (and fit uncertainty) as its average velocity. Stalling force distributions were Gaussian fitted to extract average values for single motor force production and fitted full width at half maximum were used to properly account for systematic noise. Statistical significance was determined using the Student's t-test.

Supplementary Material

Refer to Web version on PubMed Central for supplementary material.

Acknowledgements

We thank Richard McKenney for help with the quantum dot assays and useful discussion and Michael Vershinnin for developing the tracking program. This work was supported by NIH grants GM47434 to RBV, RO1GM070676 to SPG and GM008798-09 to KMOM, AHA grant 825278F to JX, and the Columbia University Motor Neuron Center.

References

1. Paschal BM, Vallee RB. Retrograde transport by the microtubule associated protein MAP 1C. Nature. 1987; 330:181–183. [PubMed: 3670402]
2. Hafezparast M, et al. Mutations in dynein link motor neuron degeneration to defects in retrograde transport. Science. 2003; 300:808–812. [PubMed: 12730604]
3. Puls I, et al. Mutant dynactin in motor neuron disease. Nat Genet. 2003; 33:455–456. [PubMed: 12627231]
4. Lai C, et al. The G59S mutation in p150(glued) causes dysfunction of dynactin in mice. J Neurosci. 2007; 27:13982–13990. [PubMed: 18094236]
5. Chevalier-Larsen ES, Wallace KE, Pennise CR, Holzbaur EL. Lysosomal proliferation and distal degeneration in motor neurons expressing the G59S mutation in the p150Glued subunit of dynactin. Hum Mol Genet. 2008; 17:1946–1955. [PubMed: 18364389]
6. Kieran D, et al. A mutation in dynein rescues axonal transport defects and extends the life span of ALS mice. J Cell Biol. 2005; 169:561–567. [PubMed: 15911875]
7. Myers KR, et al. Intermediate chain subunit as a probe for cytoplasmic dynein function: Biochemical analyses and live cell imaging in PC12 cells. J Neurosci Res. 2007; 85:2640–2647. [PubMed: 17279546]
8. Chen XJ, et al. Proprioceptive sensory neuropathy in mice with a mutation in the cytoplasmic Dynein heavy chain 1 gene. J Neurosci. 2007; 27:14515–14524. [PubMed: 18160659]
9. Ilieva HS, et al. Mutant dynein (Loa) triggers proprioceptive axon loss that extends survival only in the SOD1 ALS model with highest motor neuron death. Proc Natl Acad Sci U S A. 2008; 105:12599–12604. [PubMed: 18719118]
10. Perlson E, et al. A switch in retrograde signaling from survival to stress in rapid-onset neurodegeneration. J Neurosci. 2009; 29:9903–9917. [PubMed: 19657041]
11. King SJ, Bonilla M, Rodgers ME, Schroer TA. Subunit organization in cytoplasmic dynein subcomplexes. Protein Sci. 2002; 11:1239–1250. [PubMed: 11967380]
12. Shpetner HS, Paschal BM, Vallee RB. Characterization of the microtubule-activated ATPase of brain cytoplasmic dynein (MAP 1C). J. Cell Biol. 1988; 107:1001–1009. [PubMed: 2971069]
13. Ross JL, Wallace K, Shuman H, Goldman YE, Holzbaur EL. Processive bidirectional motion of dynein-dynactin complexes in vitro. Nat Cell Biol. 2006; 8:562–570. [PubMed: 16715075]
14. Mallik R, Carter BC, Lex SA, King SJ, Gross SP. Cytoplasmic dynein functions as a gear in response to load. Nature. 2004; 427:649–652. [PubMed: 14961123]
15. Reck-Peterson SL, et al. Single-molecule analysis of Dynein processivity and stepping behavior. Cell. 2006; 126:335–348. [PubMed: 16873064]
16. McKenney RJ, Vershinin M, Kunwar A, Vallee RB, Gross SP. LIS1 and NudE induce a persistent dynein force-producing state. Cell. 2010; 141:304–314. [PubMed: 20403325]
17. Mallik R, Petrov D, Lex SA, King SJ, Gross SP. Building complexity: an in vitro study of cytoplasmic dynein with in vivo implications. Curr Biol. 2005; 15:2075–2085. [PubMed: 16332532]
18. King SJ, Schroer TA. Dynactin increases the processivity of the cytoplasmic dynein motor. Nat Cell Biol. 2000; 2:20–24. [PubMed: 10620802]
19. Kardon JR, Reck-Peterson SL, Vale RD. Regulation of the processivity and intracellular localization of Saccharomyces cerevisiae dynein by dynactin. Proc Natl Acad Sci U S A. 2009; 106:5669–5674. [PubMed: 19293377]
20. Zhang Q, et al. Nudel promotes axonal lysosome clearance and endo-lysosome formation via dynein-mediated transport. Traffic. 2009; 10:1337–1349. [PubMed: 19522757]

21. Shubeita GT, et al. Consequences of motor copy number on the intracellular transport of kinesin-1-driven lipid droplets. Cell. 2008; 135:1098–1107. [PubMed: 19070579]
22. Hendricks AG, et al. Motor Coordination via a Tug-of-War Mechanism Drives Bidirectional Vesicle Transport. Curr Biol. 2010; 20:697–702. [PubMed: 20399099]
23. Wang Z, Khan S, Sheetz MP. Single Cytoplasmic Dynein Molecule Movements: Characterization and Comparison with Kinesin. Biophys. J. 1995; 69:2011–2023. [PubMed: 8580344]
24. Shima T, Imamula K, Kon T, Ohkura R, Sutoh K. Head-head coordination is required for the processive motion of cytoplasmic dynein, an AAA+ molecular motor. J Struct Biol. 2006; 156:182–189. [PubMed: 16677823]
25. Sweeney HL, et al. How myosin VI coordinates its heads during processive movement. EMBO J. 2007; 26:2682–2692. [PubMed: 17510632]
26. Gennerich A, Vale RD. Walking the walk: how kinesin and dynein coordinate their steps. Curr Opin Cell Biol. 2009; 21:59–67. [PubMed: 19179063]
27. Mikami A, Paschal BM, Mazumdar M, Vallee RB. Molecular cloning of the retrograde transport motor cytoplasmic dynein (MAP 1C). Neuron. 1993; 10:787–796. [PubMed: 7684232]
28. Carter BC, Shubeita GT, Gross SP. Tracking single particles: a user-friendly quantitative evaluation. Phys Biol. 2005; 2:60–72. [PubMed: 16204858]
29. Vershinin M, Carter BC, Razafsky DS, King SJ, Gross SP. Multiple-motor based transport and its regulation by Tau. Proc Natl Acad Sci U S A. 2007; 104:87–92. [PubMed: 17190808]
30. Vershinin M, Xu J, Razafsky DS, King SJ, Gross SP. Tuning microtubule-based transport through filamentous MAPs: the problem of dynein. Traffic. 2008; 9:882–892. [PubMed: 18373727]
31. Svoboda K, Schmidt CF, Schnapp BJ, Block SM. Direct observation of kinesin stepping by optical trapping interferometry. Nature. 1993; 365:721–727. [PubMed: 8413650]
32. Svoboda K, Block SM. Force and velocity measured for single kinesin molecules. Cell. 1994; 77:773–784. [PubMed: 8205624]
33. Kalafut B, Visscher K. An objective, model-independent method for detection of non-uniform steps in noisy signals. Computer Physics Communications. 2008; 179:716–723.
34. Kerssemakers JW, et al. Assembly dynamics of microtubules at molecular resolution. Nature. 2006; 442:709–712. [PubMed: 16799566]
35. Carter BC, Vershinin M, Gross SP. A comparison of step-detection methods: how well can you do? Biophys J. 2008; 94:306–319. [PubMed: 17827239]
36. Grabham PW, Bennecib M, Seale GE, Goldberg DJ, Vallee RB. Cytoplasmic Dynein and LIS1 Are Required for Growth Cone Remodeling and Fast Neurite Outgrowth. J Neurosci. 2007; 27:5823–5832. [PubMed: 17522326]

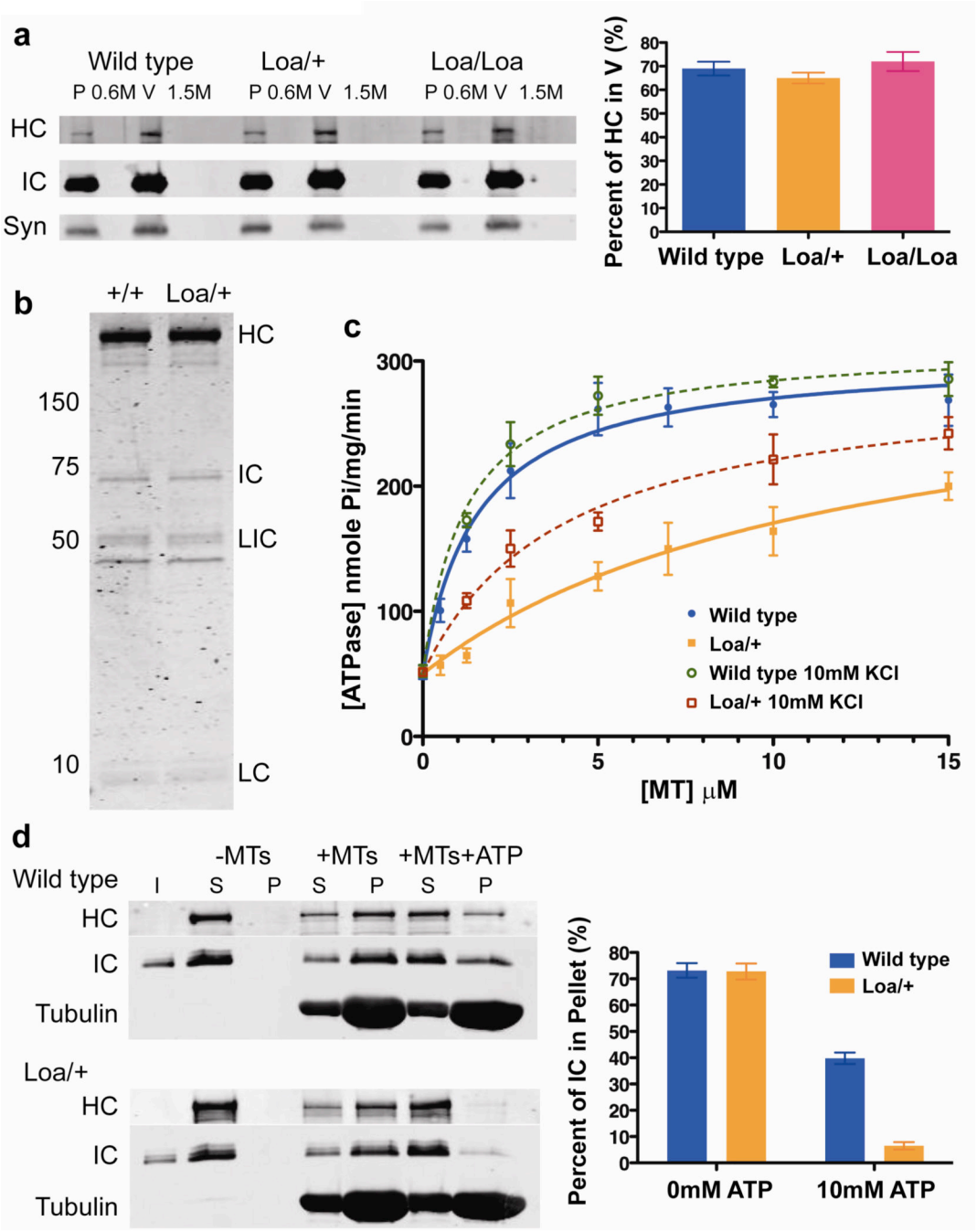

Figure 1.

Purification and biochemical analysis of wild-type and mutant cytoplasmic dynein. **(a)** Association of dynein with membrane vesicles isolated from wild-type and mutant mouse brain. Immunoblot shows comparable levels of dynein HC and IC with wild-type, Loa/+, and Loa/Loa vesicles, quantified at right (average of n = 3 experiments ± SD). P: membrane pellet; 0.6 and 1.5 M: sucrose steps; V: vesicles from sucrose interface; Syn: synaptotagmin. **(b)** Coomassie-stained gel of purified wild-type and Loa/+ brain cytoplasmic dynein. **(c)** ATPase activity of wild-type and Loa/+ dynein as a function of microtubule concentration at

low and high ionic strength. Activities ± SD were determined from n = 3 experiments in Tris buffer containing 10 mM KCl (dotted lines), or from n = 6 experiments in Tris buffer containing 50 mM KCl (dashed lines) and fitted with Michaelis-Menten kinetics. **(d)** Microtubule (MT) cosedimentation of purified wild-type and Loa/+ dynein assayed by immunoblotting for IC and tubulin. Input (I) is 20% of total. In the absence of microtubules, dynein remains in the supernatant (S). Graph depicts the amount of dynein ± SD in the microtubule pellet (P) in the absence and presence of ATP from n = 3 different experiments per genotype, per ATP condition ($P<0.001$).

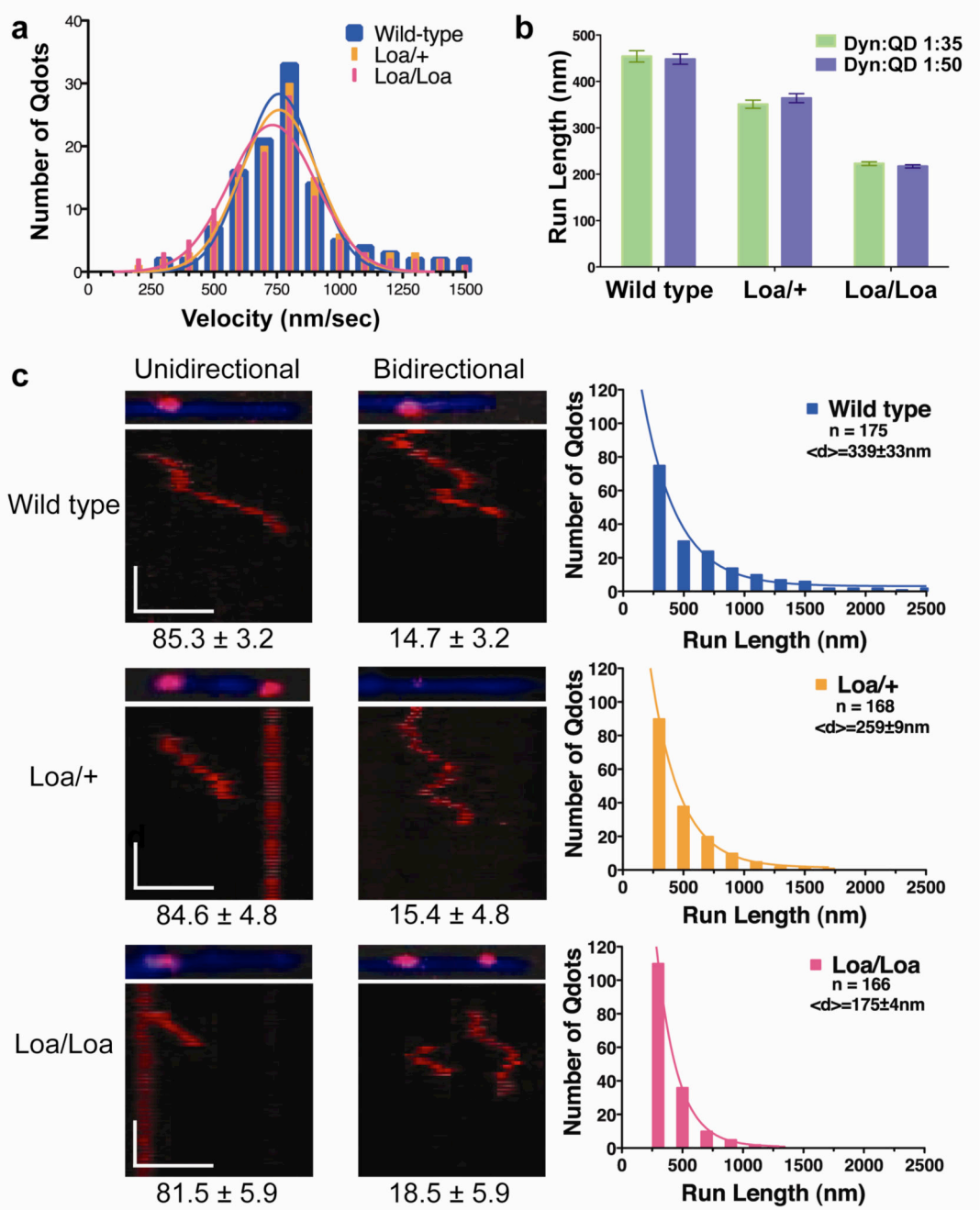

Figure 2.

Single molecule behavior of wild-type and mutant cytoplasmic dynein. Dynein was linked to quantum dots using an antibody to the IC, applied to microtubules in the absence of ATP, then monitored by fluorescence microscopy in the presence of 500 μM ATP. **(a)** Velocities for quantum dot runs > 200 nm for wild-type, Loa/+, and Loa/Loa dynein (n>111 quantum dots). **(b)** Average run-length at molar ratios of dynein:quantum dots of 1:35 and 1:50. A significant, graded reduction in run-length is observed with decreasing wild-type dynein dose (P<0.001). Error bars indicate SEM. **(c)** Kymographs of wild-type, Loa/+, and Loa/Loa

quantum dots. The percentage of quantum dots that exhibited unidirectional and bidirectional behaviors is below the kymographs. Scale bars = 1 um (x-axis) and 5 sec (y-axis). Histograms to the right of each set of kymographs depict the range of net run-lengths and associated mean ± SEM.

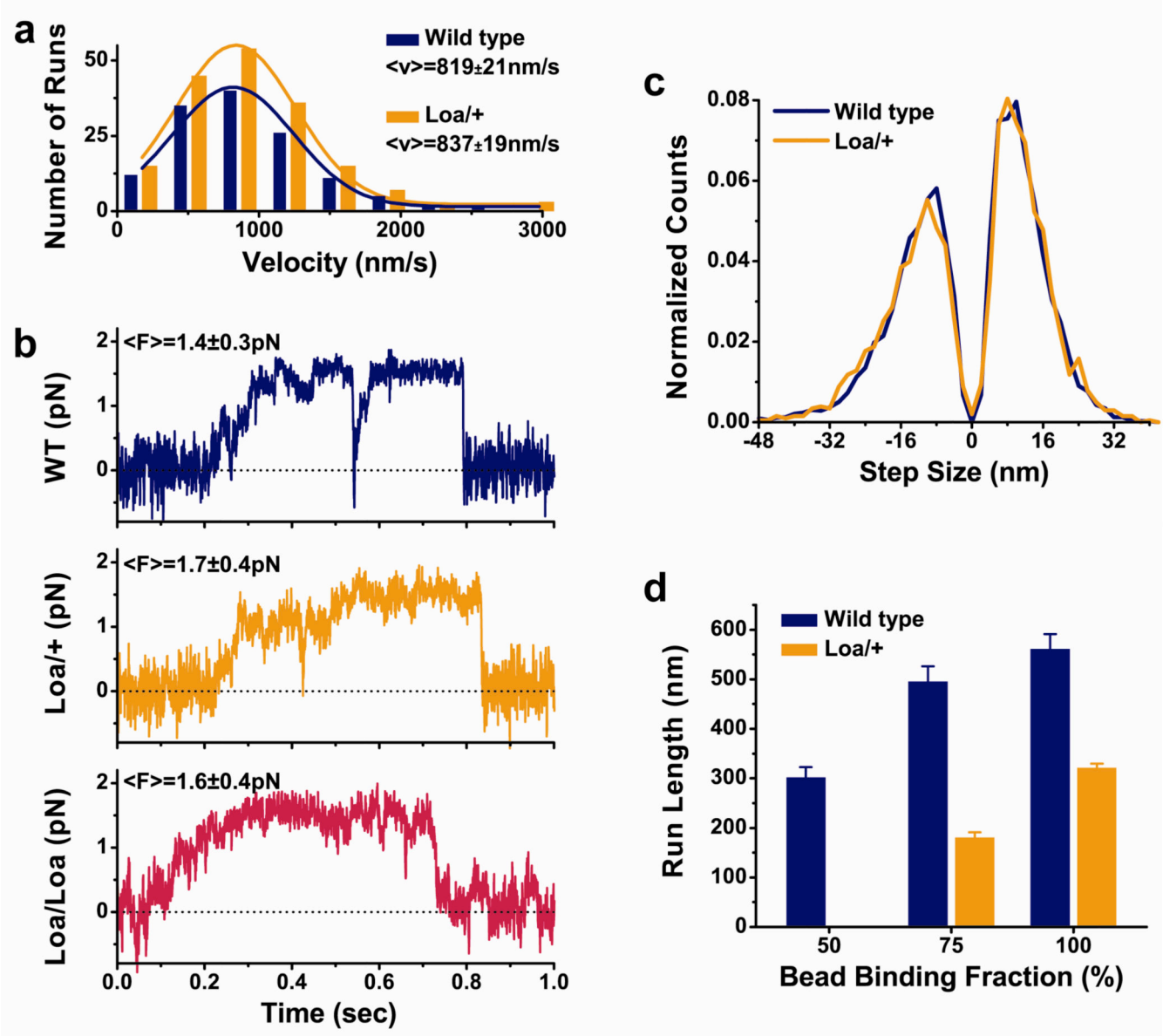

Figure 3.

Optical trap analysis of wild-type and mutant cytoplasmic dynein behavior in single- and multi-motor regions. Bead-microtubule binding fractions were used as an indicator for the average number of available motors per bead: ≤ 30 % corresponding to single motor levels and ≥ 50 % to multiple motor levels (See Supplementary Information). **(a)** Bead velocity of Loa/+ dynein is unchanged *vs.* wild-type (mean ± SEM, n > 40, *P*=0.97). **(b)** Sample single motor stall force traces reveal no significant difference between the genotypes (mean ± SD, n > 29, mean stall forces agree within systematic noise of optical trap, 0.3–0.4 pN). **(c)** Distribution of axial step sizes for wild-type and Loa/+ dynein under modest load (n > 1979, *P*=0.89). **(d)** Average run-lengths in modest multi-motor range of Loa/+ dyneins are significantly reduced from that of wild-type motors. Error bars represent the SEM (wild-type: n = 38, 64, and 127 runs for binding fraction of 50, 75, and 100 %, respectively;

Loa/+: n = 39 and 296 runs for binding fraction of 75 and 100 %, respectively. $P<0.03$). Loa/+ run-length at 50 % binding fraction was below measurement limit under assay conditions used here (Fig. S4c).

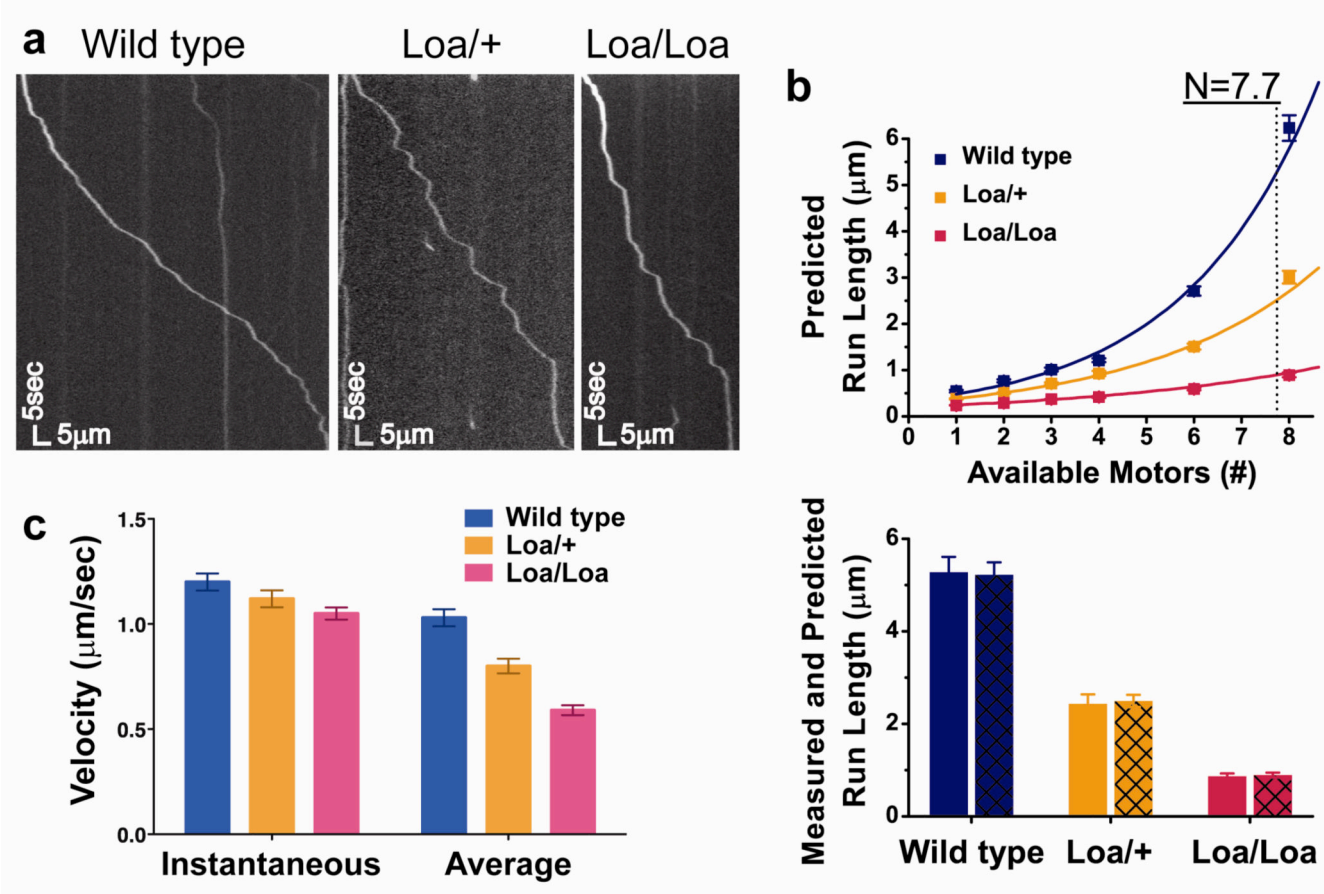

Figure 4.

Analysis of retrograde transport of lysosomes in wild-type and mutant axons, with theoretical comparison. (**a**) Kymographs of retrograde transport of lysosomes in axons, representative of more processive lysosome runs. (**b**) Theory (top) was constrained with wild-type data (blue arrow) to predict motor number (dotted line), and then predict mutant run-lengths for mutant dynein (orange and pink arrows) (mean ± SEM, n > 400, 300, 600 simulated runs for wild type, Loa/+ and Loa/Loa, respectively). We find striking agreement between predictions (using 7.7 as the number of available motors) and *in vivo* measurements (bottom, hatched *vs.* solid bars, respectively). Error bars represent the SEM (n = 68, 78, and 55 uninterrupted retrograde runs for wild type, Loa/+ and Loa/Loa, respectively). (**c**) Graph depicting instantaneous and average lysosome velocities ± SEM for each genotype (n = 102, 98, and 111 for wild type, Loa/+ and Loa/Loa, respectively, $P<0.001$ for run-length and average velocity).

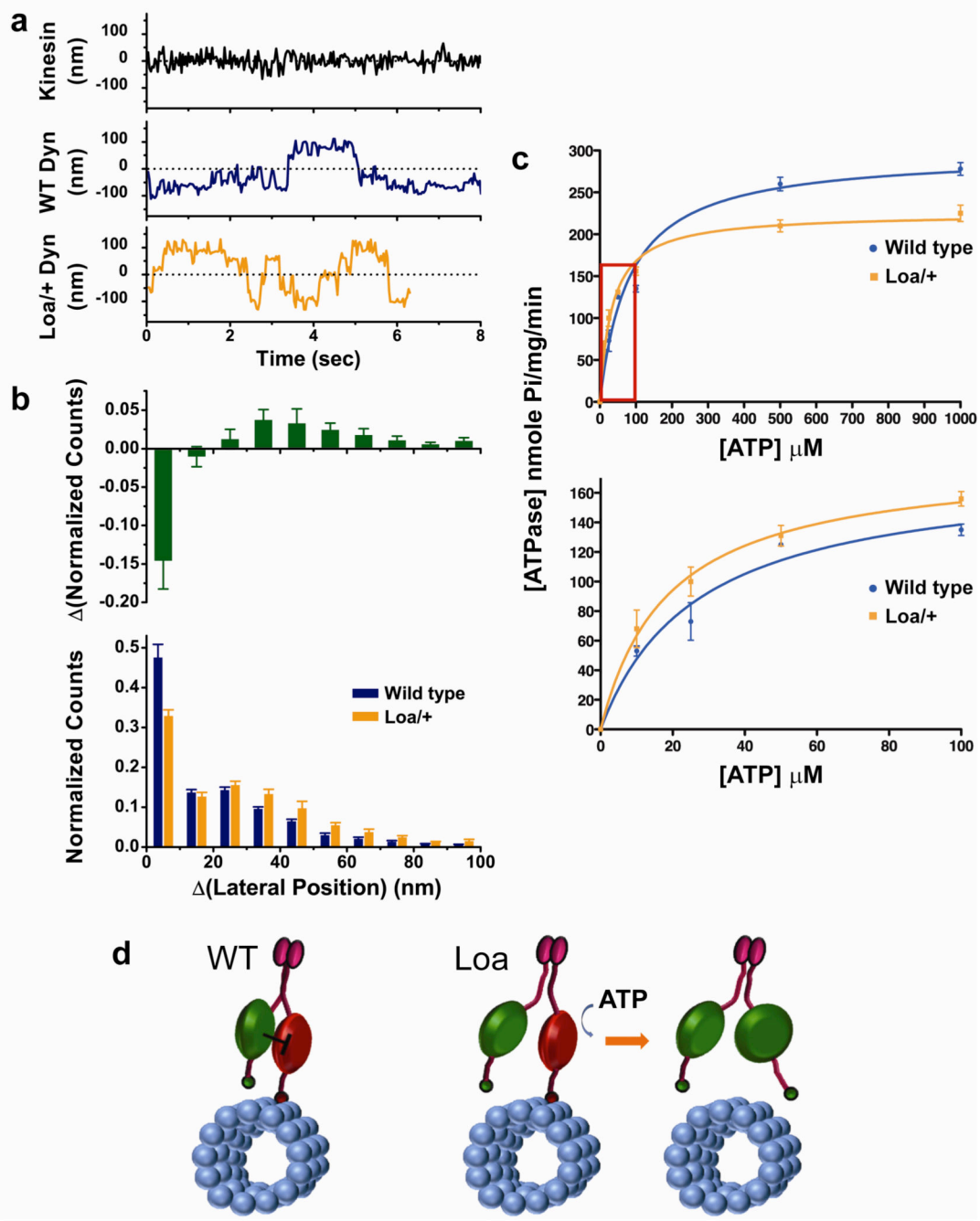

Figure 5.

Biophysical and biochemical evidence of altered motor coordination in mutant dynein. **(a)** Sample lateral position traces of beads carried by a single kinesin, wild-type or Loa/+ dynein. **(b)** Distributions of the instantaneous change in lateral position for dynein (bottom) demonstrates a significant deviation of mutant dynein from wild-type (top) (n = 32 and 18 runs for wild-type and Loa/+, respectively; $P<0.05$). Error bars represent the SD. **(c)** ATP concentration dependence of wild-type and Loa/+ dynein ATPase activity at 10 μM microtubules. Low ATP concentration range is expanded in bottom graph. Activities ± SD

were determined from three different experiments per genotype and fitted to Michaelis-Menten kinetics. **(d)** Proposed effect of Loa mutation on motor coordination. In wild-type dynein, the stepping head (green) inhibits the tightly bound head (red) from binding ATP. In Loa dynein, the stepping head (green) does not adequately inhibit the tightly bound head (red), which binds ATP prematurely and causes release from the microtubule.